Available online at www.sciencedirect.com
ScienceDirect
Journal of Sound and Vibration 321 (2009) 1007–1025
JOURNAL OF SOUND AND VIBRATION
www.elsevier.com/locate/jsvi

Volume-to-surface reduction of vorticoacoustic stability integrals

Sean R. Fischbach[1], Joseph Majdalani*

Department of Mechanical, Aerospace and Biomedical Engineering, The University of Tennessee (UTSI), 411 B.H. Goethert Parkway, MS-23, Tullahoma, TN 37388-9700, USA

Received 6 May 2007; received in revised form 6 June 2008; accepted 3 October 2008
Handling Editor: S. Bolton
Available online 28 November 2008

Abstract

It is generally accepted that incorporation of unsteady rotational sources and sinks into the acoustic energy balance equation leads to a more precise assessment of acoustic instability in rocket chambers. The process involves the calculation of 10 acoustic growth rate terms that arise in the context of an oscillating flow in an idealized rocket chamber; the chamber is modelled as an injection-driven enclosure with coupling along its porous walls between acoustical and vortical waves. In this study, we convert the 10 stability integrals from volume to surface form. The surface integrals are then verified using numerical comparisons for three baseline cases that span a practical range of solid rocket motors. The surface integrals are further reduced and presented in a strictly acoustical form that is directly amenable to implementation in the standard stability prediction program. This code devotes itself to the assessment of acoustic energy in rocket motors. The reduction to surface form facilitates the evaluation of individual stability growth rates as each becomes a function of quantities that are distributed along the chamber's boundaries. By obviating the need to compute the rotational field (which is the most difficult to capture, especially in complex geometry), the evaluation of acoustic stability integrals is simplified for motors with variable grain configuration.

1. Introduction

Combustion instability is a long-standing problem that was first observed in the test firings of solid rocket motors in the 1930s. Given the limited resources available for measuring the high frequency pressure oscillations that accompanied the onset of instability, early diagnostic tools were based on simple detection methods. These included visual inspection and interpretation of irregular exhaust plumes, rippled conduits, and the auditory tones produced during motor firings. As technology progressed and experimental capabilities improved, combustion instability became identifiable from its large amplitude pressure excursions and the particular spectra that it engendered.

*Corresponding author. Tel.: +1 931 393 7280; fax: +1 931 393 7530.
E-mail addresses: Sean.R.Fischbach@nasa.gov (S.R. Fischbach), maji@utsi.edu (J. Majdalani).
[1]Present address: Acoustic and Stability Engineer, Qualis Corporation, NASA Marshall Space Flight Center, Huntsville, AL 35812, USA.

0022-460X/$ - see front matter © 2008 Elsevier Ltd. All rights reserved.
doi:10.1016/j.jsv.2008.10.001

From its earliest beginnings, the modelling of combustion instability mechanisms received attention from a number of capable investigators. A short list would include Crocco and Cheng [1,2], Sirignano and Crocco [3], Mitchell [4], Zinn [5], Culick [6], and Flandro [7–10]. These researchers have attempted, in a series of evolutionary studies, to apply mechanistic approaches to capture and predict essential combustion instability behaviour.

Hart and McClure [11,12] were perhaps the first to evoke the concept of an energy balance equation in assessing motor stability. Their approach, however, did not attempt to decompose unsteady energy into its irrotational (compressible) and rotational (solenoidal) parts. Later investigators employed a variety of experimental [13–16], numerical [17–24], and analytical methods to explore particular aspects of this problem (e.g. Refs. [25–42]). The present analysis serves to extend the general energy method that was introduced in 1959 and later enhanced in 1985 [10].

Following similar lines to those sketched by Hart and McClure [11,12], Flandro and Majdalani [43], and Majdalani et al. [33] have shown that, by incorporating unsteady rotational terms into the acoustic energy equation, a more accurate estimation procedure for the progression of internal energy in rocket motors can be obtained. In subsequent studies [33,34], their multidimensional approach was confirmed and extended to other geometry [22–24].

The multidimensional energy assessment involves both rotational and irrotational contributions to the instantaneous pressure and velocity fields (p, $\mathbf{u}$) in an elongated chamber. As a result of retaining the effects of unsteady vorticity, the predictive formulation gives rise to 10 volume integrals representing distinct acoustico-vortical mechanisms affecting stability. In previous work [33,34], these 10 integrals have been classified and characterized according to their physical significance. In short, they may be expanded into a series of individual factors that can be aggregated to obtain the total linear instability growth rate, α_m. This is given by $\alpha_m = \alpha_1 + \alpha_2 + \alpha_3 + \cdots$.

In this work, the focus will be on the linear growth rate α_m and the conversion of its constituents from volume to surface integral form. This operation requires the application of surface treatment, several vector theorems, the no slip condition at the porous walls, and other boundary related responses, to the 10 stability factors. The conversion to surface form will be shown to markedly improve the practical evaluation of these predictive integrals. At the outset, calculations will no longer be dependent on the complex fluid flow interactions inside the motor, particularly when the mode shapes and frequencies can be obtained analytically or numerically. By taking advantage of surface coupling between acoustical and rotational flow variables, the rotational components will be nearly eliminated from the analysis. Not only will the resulting growth rates be expressible in surface integral form, but they will also be made mostly dependent on acoustic variables. The final form will be incorporated into the existing acoustic code. By way of confirmation, French et al. [22] will then show that their adaptation yields better agreement with available measurements.

The present article comprises two main sections: analysis and verification. At first, the acoustic stability integrals that have been previously derived in volume form [33,43] are systematically converted to surface form. Next, the resulting expressions are verified for the case of a full-length, internal burning, cylindrical chamber. The idealized, circular-port chamber is routinely used by Blomshield and Mathes [13], Bloomshield et al. [14,15], Fabignon et al. [16], Chedevergne et al. [44], and others.

2. Analysis

2.1. Energy assessment

Our study considers the geometry and nomenclature adopted in several studies of the circular-port motor shown in Fig. 1 [8,43]. The evolution of the system energy (E) with rotational corrections in an injection-driven porous enclosure was developed by Flandro and Majdalani [43] and later refined in Ref. [33]. The description of acoustico-vortical wave components was obtained in different chambers by Flandro [45], Majdalani and Flandro [46], and Majdalani [39–42]. Using similar nomenclature, our starting point is the time rate of change of the acoustic energy E that retains both vorticity-driven, rotational ($\sim$) and pressure-driven, irrotational ($\hat{}$)

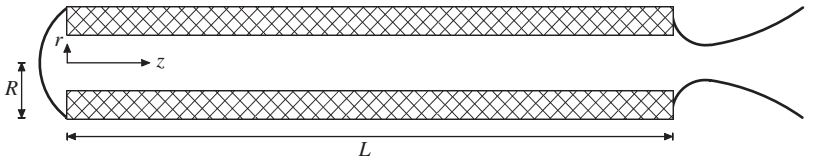

Fig. 1. Full-length grain geometry and coordinate system.

components of velocity $\mathbf{u}$ and pressure p. This expression is

$$\frac{\mathrm{d}E}{\mathrm{d}t}= \left.\begin{array}{c} \iiint_V \big\langle -\nabla\cdot(\hat{p}\hat{\mathbf{u}}) - \tfrac{1}{2}M_b(\mathbf{U}\cdot\nabla\hat{p}^2) - M_b[\hat{\mathbf{u}}\cdot\nabla(\mathbf{U}\cdot\hat{\mathbf{u}})] + \tfrac{4}{3}\delta^2\hat{\mathbf{u}}\cdot\nabla(\nabla\cdot\hat{\mathbf{u}}) \\ +M_b[\hat{\mathbf{u}}\cdot(\hat{\mathbf{u}}\times\boldsymbol{\Omega}) + \hat{\mathbf{u}}\cdot(\mathbf{U}\times\boldsymbol{\omega})] - \tilde{\mathbf{u}}\cdot\nabla\hat{p} \\ -M_b[\tilde{\mathbf{u}}\cdot\nabla(\mathbf{U}\cdot\hat{\mathbf{u}}) + \hat{\mathbf{u}}\cdot\nabla(\mathbf{U}\cdot\tilde{\mathbf{u}}) + \tilde{\mathbf{u}}\cdot\nabla(\mathbf{U}\cdot\tilde{\mathbf{u}}) - \tilde{\mathbf{u}}\cdot(\mathbf{U}\times\boldsymbol{\omega}) - \tilde{\mathbf{u}}\cdot(\tilde{\mathbf{u}}\times\boldsymbol{\Omega})] \\ +\tfrac{4}{3}\delta^2\tilde{\mathbf{u}}\cdot\nabla(\nabla\cdot\hat{\mathbf{u}}) - \delta^2[\hat{\mathbf{u}}\cdot(\nabla\times\boldsymbol{\omega}) + \tilde{\mathbf{u}}\cdot(\nabla\times\boldsymbol{\omega})] - \hat{\mathbf{u}}\cdot\nabla\tilde{p} - \tilde{\mathbf{u}}\cdot\nabla\tilde{p}\big\rangle\,\mathrm{d}V. \end{array}\right\} \tag{1}$$

In the above, the surface Mach number is defined as $M_b = V_b/a_0$, where V_b is the wall blowing velocity and a_0 is the average speed of sound. Viscous effects are reflected in the viscous parameter $\delta = [\nu/(a_0 R)]^{1/2}$ with the kinematic viscosity being $\nu = \mu/\rho$ and R denoting the chamber radius. The chamber volume is designated by $V = \pi R^2 L$ with r, z, t being the radial, axial and temporal coordinates, respectively. This study utilizes the incompressible Taylor–Culick mean flow profile $\mathbf{U}$ [35], where

$$\mathbf{U} = U_r\mathbf{e}_r + U_z\mathbf{e}_z = -r^{-1}\sin(x)\mathbf{e}_r + \pi z\cos(x)\mathbf{e}_z. \tag{2}$$

Here $x \equiv \frac{1}{2}\pi r^2$ while $\mathbf{e}_r$ and $\mathbf{e}_z$ denote the unit vectors in the r and z directions. In Eq. (1), ω and Ω represent the unsteady and mean vorticity magnitudes. The stability integrals to be converted will repeatedly refer to Eq. (1). The unsteady pressure and velocities represented in Eq. (1) are for longitudinal plane waves that are expressible via [34]

$$\hat{p} = \hat{p}_m\exp(\alpha_m t)\cos(k_m t), \quad \hat{p}_m = \cos(k_m z) \quad \text{(acoustic pressure mode shape)}, \tag{3}$$

$$\hat{\mathbf{u}} = \hat{\mathbf{u}}_m\exp(\alpha_m t)\sin(k_m t), \quad \hat{\mathbf{u}}_m = \sin(k_m z)\mathbf{e}_z \quad \text{(acoustic velocity mode shape)}, \tag{4}$$

and, for the rotational parts,

$$\tilde{p} = \exp(\alpha_m t)[\tilde{p}^r_m\cos(k_m t) + \tilde{p}^i_m\sin(k_m t)], \quad \left.\begin{array}{l} \tilde{p}^r_m = -\tfrac{1}{2}\pi M_b z\sin(\psi)\sin(2x)\exp(\phi)\sin[k_m z\sin(x)] \\ \tilde{p}^i_m = \tfrac{1}{2}\pi M_b z\cos(\psi)\sin(2x)\exp(\phi)\sin[k_m z\sin(x)] \end{array}\right\}, \tag{5}$$

$$\tilde{\mathbf{u}} = \exp(\alpha_m t)[\tilde{\mathbf{u}}^r_m\cos(k_m t) + \tilde{\mathbf{u}}^i_m\sin(k_m t)], \quad \left.\begin{array}{l} \tilde{\mathbf{u}}^r_m = \sin(x)\exp(\phi)\sin(\psi)\sin[\sin(x)k_m z]\mathbf{e}_z \\ \tilde{\mathbf{u}}^i_m = -\sin(x)\exp(\phi)\cos(\psi)\sin[\sin(x)k_m z]\mathbf{e}_z \end{array}\right\}, \tag{6}$$

with the superscript r and i depicting the real and imaginary parts of a complex exponential. In the above $k_m = m\pi/l$ represents the dimensionless wavenumber of the mth axial acoustic mode in a chamber of aspect ratio $l = L/R$ (Fig. 1). The remaining arguments and parameters include

$$\phi(r) = \frac{\xi}{\pi^2}\left[1 - \frac{1}{\sin(x)} - x\frac{\cos(x)}{\sin^2(x)} + I(x) - I\left(\tfrac{1}{2}\pi\right)\right], \quad \psi(r) = -\frac{k_m}{\pi M_b}\ln\tan\left(\tfrac{1}{2}x\right), \tag{7}$$

where

$$I(x) \equiv \int_0^x \eta\csc\eta\,\mathrm{d}\eta = x + \frac{1}{18}x^3 + \frac{7}{1800}x^5 + \frac{31}{105\,840}x^7 + O(x^9). \tag{8}$$

Note that $\xi = k_m^2\delta^2/M_b^3$ is a dimensionless group parameter representing the relative effects of viscosity with respect to unsteady inertia [47], and $S = k_m/M_b$ is the Strouhal number [37].

The unsteady energy density for this vortico-acoustic field may be obtained after Kirchoff [48], namely,

$$e = \tfrac{1}{2}[\hat{p}^2 + \mathbf{u}^{(1)} \cdot \mathbf{u}^{(1)}]; \quad \mathbf{u}^{(1)} = \hat{\mathbf{u}} + \tilde{\mathbf{u}}. \tag{9}$$

Realizing that the energy transfer mechanism unfolds more slowly than the oscillation mechanism, the characteristic time scale for energy transfer may be chosen to be much larger than the period of oscillation. Time averaging may be carried out by averaging over the period of oscillation. The energy density is also averaged over the chamber volume V, thus leading to

$$E = \iiint_V \langle e \rangle \, \mathrm{d}V = \frac{1}{2} \iiint_V \langle \hat{p}^2 + \mathbf{u}^{(1)} \cdot \mathbf{u}^{(1)} \rangle \, \mathrm{d}V. \tag{10}$$

Inserting the unsteady field into the foregoing equations enables us to write

$$\langle e \rangle = \frac{1}{4} \exp(2\alpha_m t) \left[\overbrace{\hat{p}_m^2 + \hat{\mathbf{u}}_m \cdot \hat{\mathbf{u}}_m}^{\text{irrotational}} + \overbrace{2\hat{\mathbf{u}}_m \cdot \tilde{\mathbf{u}}_m^i + \tilde{\mathbf{u}}_m^r \cdot \tilde{\mathbf{u}}_m^i + \tilde{\mathbf{u}}_m^i \cdot \tilde{\mathbf{u}}_m^i}^{\text{rotational}} \right]. \tag{11}$$

Then, since

$$\frac{\mathrm{d}E}{\mathrm{d}t} = \alpha_m \exp(2\alpha_m t) E_m^2, \quad \alpha_m = \sum_{i=1}^{N} \alpha_i, \tag{12}$$

the energy normalization function E_m^2 may be retrieved. One obtains $E_m^2 = \frac{5}{8}\pi L/R$ for an internal burning cylindrical chamber. In general, as shown in detail by Majdalani et al. [34], E_m^2 can be derived from

$$E_m^2 = \frac{1}{2} \iiint_V (\hat{p}_m^2 + \hat{\mathbf{u}}_m \cdot \hat{\mathbf{u}}_m + 2\hat{\mathbf{u}}_m \cdot \tilde{\mathbf{u}}_m^i + \tilde{\mathbf{u}}_m^r \cdot \tilde{\mathbf{u}}_m^r + \tilde{\mathbf{u}}_m^i \cdot \tilde{\mathbf{u}}_m^i) \, \mathrm{d}V. \tag{13}$$

2.2. Integral conversion

2.2.1. Pressure coupling and nozzle damping integral

The extended pressure coupling correction factor combines the first three irrotational integrals that appear in Eq. (1). These represent pressure coupling and nozzle damping due to the acoustic energy being transported away by the mean flow field. Using standard arguments, the corresponding energy growth rate may be determined to be

$$\alpha_1 = \frac{E_m^{-2}}{\exp(2\alpha_m t)} \iiint_V \left\langle -\nabla \cdot \left[\hat{p}\hat{\mathbf{u}} + \frac{1}{2} M_b \mathbf{U} (\hat{p})^2 \right] - M_b [\hat{\mathbf{u}} \cdot \nabla (\mathbf{U} \cdot \hat{\mathbf{u}})] \right\rangle \mathrm{d}V. \tag{14}$$

The divergence theorem can be directly applied to the first term on the right-hand-side of Eq. (14). The second term, however, requires the use of vector identities and the rewriting of the unsteady velocities in terms of the unsteady pressure [33]. At the outset, Eq. (14) becomes

$$\begin{aligned} \alpha_1 = {} & \frac{1}{4} M_b E_m^{-2} \left\{ \iint_{S_b} \cos^2(k_m z) \, \mathrm{d}S - \iint_{S_N} U_N \cos^2(k_m z) \, \mathrm{d}S \right\} \\ & + \frac{1}{2} M_b E_m^{-2} \left(\iint_{S_b} \left\{ \cos^2(k_m z) \left[A_b^{(r)} + \frac{1}{2} \right] \right\} \mathrm{d}S - \iint_{S_N} \left\{ \cos^2(k_m z) \left[A_N^{(r)} + \frac{1}{2} U_N \right] \right\} \mathrm{d}S \right), \end{aligned} \tag{15}$$

where S_b and S_N refer to the porous sidewall and nozzle entrance plane, respectively. Moreover, $A_b^{(r)} = -\mathbf{n} \cdot \hat{\mathbf{u}}/(M_b \hat{p})$ is the burning surface admittance, $A_N^{(r)} = \mathbf{n} \cdot \hat{\mathbf{u}}/(M_b \hat{p})$ is the nozzle entrance plane admittance,

and U_N is the mean flow velocity in the nozzle entrance plane. Collecting similar integrals, one obtains

$$\alpha_1 = \frac{1}{2} M_b E_m^{-2} \iint_{S_b} \cos^2(k_m z)[A_b^{(r)} + 1]\,\mathrm{d}S - \frac{1}{2} M_b E_m^{-2} \iint_{S_N} \cos^2(k_m z)[A_N^{(r)} + U_N]\,\mathrm{d}S. \tag{16}$$

In more general form, α_1 can be expressed as

$$\alpha_1 = \frac{1}{2} M_b E_m^{-2} \iint_{S_b} \hat{p}_m^2[A_b^{(r)} + 1]\,\mathrm{d}S - \frac{1}{2} M_b E_m^{-2} \iint_{S_N} \hat{p}_m^2[A_N^{(r)} + U_N]\,\mathrm{d}S. \tag{17}$$

For a circular-port motor, α_1 reduces to $\alpha_1 = \frac{4}{5} M_b[A_b^{(r)} - \gamma]$, with γ being the ratio of specific heats.

2.2.2. Dilatational energy integral

The second correction stems from the fourth irrotational term in Eq. (1) and is known as the dilatational energy term. It is shown in previous studies that, being of $O(M_b^3)$, α_2 may be discounted [33]. For further confirmation, one may start from

$$\alpha_2 = E_m^{-2} \exp(-2\alpha_m t) \iiint_V \left\langle \frac{4}{3} \delta^2 \hat{\mathbf{u}} \cdot \nabla(\nabla \cdot \hat{\mathbf{u}}) \right\rangle \mathrm{d}V. \tag{18}$$

One may then apply time averaging to get

$$\alpha_2 = \frac{2}{3} E_m^{-2} \iiint_V \delta^2 \hat{\mathbf{u}}_m \cdot \nabla(\nabla \cdot \hat{\mathbf{u}}_m)\,\mathrm{d}V. \tag{19}$$

Then using $\nabla \cdot \hat{\mathbf{u}}_m = k_m \hat{p}_m$ and $\nabla \hat{p}_m = -k_m \hat{\mathbf{u}}_m$, one extracts

$$\alpha_2 = \frac{2}{3} E_m^{-2} \iiint_V \delta^2(-\nabla \hat{p}_m / k_m) \cdot \nabla(k_m \hat{p}_m)\,\mathrm{d}V = -\frac{2}{3} \delta^2 E_m^{-2} \iiint_V (\nabla \hat{p}_m \cdot \nabla \hat{p}_m)\,\mathrm{d}V. \tag{20}$$

Additionally, one may use vector identities to deduce

$$\alpha_2 = -\frac{2}{3} \delta^2 E_m^{-2} \iiint_V [\nabla \cdot (\hat{p}_m \nabla \hat{p}_m) + k_m^2 \hat{p}_m^2]\,\mathrm{d}V. \tag{21}$$

In both experimental tests and numerical simulations, acoustic modes are found to dominate. One may therefore use the standard approximation adopted by Culick [49] and others, namely,

$$E_m^2 = \frac{1}{2} \iiint_V \hat{p}_m^2\,\mathrm{d}V.$$

Eq. (21) becomes

$$\alpha_2 = -\frac{2}{3} \delta^2 E_m^{-2} \left[\iiint_V \nabla \cdot (\hat{p}_m \nabla \hat{p}_m)\,\mathrm{d}V + 2k_m^2 E_m^2 \right]. \tag{22}$$

The divergence theorem may now be applied along with the evaluation of the normal projections. One is left with

$$\alpha_2 = -\frac{2}{3} \delta^2 k_m E_m^{-2} \left[\iint_{S_b} M_b A_b^{(r)} \hat{p}_m^2\,\mathrm{d}S - \iint_{S_N} M_b A_N^{(r)} \hat{p}_m^2\,\mathrm{d}S \right] - \frac{4}{3} \delta^2 k_m^2. \tag{23}$$

When evaluated for a circular-port motor, α_2 reduces to

$$\alpha_2 = -\tfrac{8}{15}\xi M_b^3 - \tfrac{16}{15}\xi M_b^4 k_m^{-1}(A_b^r - \gamma - 1) = -\tfrac{8}{15}\xi M_b^3[1 + 2S^{-1}(A_b^r - \gamma - 1)]. \tag{24}$$

This factor is relatively small due to its dependence on ξM_b^3, an exceedingly small quantity [31].

2.2.3. Acoustic mean flow integral

By turning attention to the third growth rate factor, one finds

$$\alpha_3 = E_m^{-2}\exp(-2\alpha_m t)\iiint_V \langle M_b\{\hat{\mathbf{u}}\cdot(\hat{\mathbf{u}}\times\boldsymbol{\Omega})\}\rangle\,\mathrm{d}V \equiv 0. \tag{25}$$

This term vanishes because $\hat{\mathbf{u}}\times\boldsymbol{\Omega}$ is perpendicular to $\hat{\mathbf{u}}$, $\forall\boldsymbol{\Omega}$.

2.2.4. Flow turning integral

The fourth factor connotes *the flow turning correction* [43] and is the first to depend on unsteady vorticity. Starting with

$$\alpha_4 = E_m^{-2}\,\mathrm{e}^{-2\alpha_m t}\iiint_V \langle M_b\hat{\mathbf{u}}\cdot(\mathbf{U}\times\boldsymbol{\omega})\rangle\,\mathrm{d}V, \tag{26}$$

the integrand may be expanded by recognizing that the vorticity is a function of the unsteady rotational velocity, $\boldsymbol{\omega} = \nabla\times\tilde{\mathbf{u}}$. Then, recalling that the unsteady flow is axisymmetric and that the acoustic velocity has no radial or tangential components, one may insert $\partial\tilde{u}_r/\partial z = O(M_b^2)$ into the integrand to obtain

$$\hat{\mathbf{u}}\cdot(\mathbf{U}\times\boldsymbol{\omega}) = -\hat{u}_z U_r\frac{\partial\tilde{u}_z}{\partial r}. \tag{27}$$

At this juncture it is advantageous to substitute the values for $\tilde{u}_z$, U_r and $\hat{u}_z$ to retrieve

$$\hat{\mathbf{u}}\cdot(\mathbf{U}\times\boldsymbol{\omega}) = \sin(k_m z)\,\mathrm{e}^{2\alpha_m t}\,\sin(k_m t)r^{-1}\,\sin(x)\left[\frac{\partial\tilde{u}_m^r}{\partial r}\cos(k_m t) + \frac{\partial\tilde{u}_m^i}{\partial r}\sin(k_m t)\right]. \tag{28}$$

In order to simplify Eq. (28), time averaging must be performed. One gets

$$\alpha_4 = -\frac{1}{2}M_b E_m^{-2}k_m^{-1}\iiint_V r^{-1}\,\sin(x)\frac{\partial\tilde{u}_m^i}{\partial r}\,\nabla\hat{p}_m\,\mathrm{d}V, \tag{29}$$

where

$$r^{-1}\,\sin(x)\frac{\partial\tilde{u}_m^i}{\partial r}\nabla\hat{p}_m \approx \frac{\partial}{\partial r}(-U_r\tilde{\mathbf{u}}_m^i\cdot\nabla\hat{p}_m). \tag{30}$$

This approximation is valid due to the unsteady vorticity being $O(M_b{}^{-1})$ [46]. The radial part of the integral may be determined entirely from the upper limit at $r = 1$. The volume integral, noting that $U_r(1) = -1$, may be replaced by a surface integral of the form

$$\alpha_4 = \frac{1}{2}M_b E_m^{-2}\iint_{S_b}\tilde{\mathbf{u}}_m^i\cdot\hat{\mathbf{u}}_m\,\mathrm{d}S. \tag{31}$$

The non-time-averaged form of Eq. (31) is clearly

$$\alpha_4 = \exp(-2\alpha_m t)M_b E_m^{-2}\iint_{S_b}\langle\tilde{\mathbf{u}}^i\cdot\hat{\mathbf{u}}\rangle\,\mathrm{d}S. \tag{32}$$

Note that this integral is only defined over the burning surface; it is not to be evaluated over inert sections or the nozzle entrance region. For a circular-port motor α_4 reduces to

$$\alpha_4 = -\tfrac{4}{5}M_b. \tag{33}$$

2.2.5. Rotational flow integral

The next rotational flow correction is the fifth growth rate factor and represents the first of the new terms introduced by Flandro and Majdalani [43]. This correction stems from the convection of acoustic pressure by virtue of the three-dimensional rotational velocity. From Eq. (1), the first of the rotational integrals yields

$$\alpha_5 = -E_m^{-2}\exp(-2\alpha_m t)\iiint_V \langle \tilde{\mathbf{u}}\cdot\nabla\hat{p}\rangle\,\mathrm{d}V = -E_m^{-2}\exp(-2\alpha_m t)\iiint_V \langle \nabla\cdot(\tilde{\mathbf{u}}\hat{p})\rangle\,\mathrm{d}V, \tag{34}$$

where vector identities have been used. At this point, α_5 may be readily converted to surface form by direct application of the divergence theorem; one gets

$$\alpha_5 = -E_m^{-2}\exp(-2\alpha_m t)\iint_S \langle \mathbf{n}\cdot(\tilde{\mathbf{u}}\hat{p})\rangle\,\mathrm{d}S, \tag{35}$$

with $\mathbf{n}$ being the outward pointing vector normal to the boundaries. Time averaging is subsequently applied along with the evaluation of applicable normal projections to produce, for a circular-port motor,

$$\alpha_5 = \frac{1}{2}E_m^{-2}\iint_{S_b} M_b\hat{p}_m^2\,\mathrm{d}S \approx \frac{4}{5}M_b. \tag{36}$$

It may be interesting to note that α_4 and α_5 cancel when converted to surface form and then evaluated for the full-length, internal burning cylinder. This result was first emphasized by Flandro and Majdalani [50] when the cancellation occurred as they evaluated the volume integrals associated with this particular configuration.

2.2.6. Inviscid vortical integral

The sixth factor is dubbed the mean vortical correction [33]; it is given by

$$\alpha_6 = E_m^{-2}\exp(-2\alpha_m t)\iiint_V \langle M_b\tilde{\mathbf{u}}\cdot(\mathbf{U}\times\boldsymbol{\omega})\rangle\,\mathrm{d}V. \tag{37}$$

The conversion of α_6, being elaborate, is partly consigned to Appendix A. The outcome is

$$\alpha_6 = -M_b E_m^{-2}\exp(-2\alpha_m t)\iint_S \left\langle \mathbf{n}\cdot\left[\mathbf{U}\left(\frac{1}{2}\tilde{\mathbf{u}}\cdot\tilde{\mathbf{u}}\right)\right]\right\rangle \mathrm{d}S. \tag{38}$$

This expression may be further simplified by expanding the rotational unsteady velocity into a tangential and a wall-normal component (i.e., radial in a cylindrical chamber). Thus, using

$$\tilde{\mathbf{u}} = (\mathbf{n}\cdot\tilde{\mathbf{u}})\mathbf{n} + [\tilde{\mathbf{u}} - (\mathbf{n}\cdot\tilde{\mathbf{u}})\mathbf{n}], \tag{39}$$

one recognizes that the tangential rotational component will satisfy the no-slip condition by identically offsetting the irrotational velocity at the surface; hence

$$\tilde{\mathbf{u}} - (\mathbf{n}\cdot\tilde{\mathbf{u}})\mathbf{n} = -[\hat{\mathbf{u}} - (\mathbf{n}\cdot\hat{\mathbf{u}})\mathbf{n}]. \tag{40}$$

As shown in Ref. [46], the unsteady rotational velocity $(\mathbf{n}\cdot\tilde{\mathbf{u}})\mathbf{n}$ that affects our calculations is negligible in the exit plane, being situated near a velocity node. Evaluation over the head wall or nozzle surface S_N may hence be ignored. As the surface conversion is carried out over the burning surface S_b, one may substitute $\mathbf{n}\cdot\tilde{\mathbf{u}} = -M_b\hat{p}$. This turns Eq. (39) into

$$\tilde{\mathbf{u}} = -M_b\hat{p}\mathbf{n} - [\hat{\mathbf{u}} - (\mathbf{n}\cdot\hat{\mathbf{u}})\mathbf{n}] = (-M_b\hat{p} + \mathbf{n}\cdot\hat{\mathbf{u}})\mathbf{n} - \hat{\mathbf{u}}, \tag{41}$$

and so

$$\tilde{\mathbf{u}}\cdot\tilde{\mathbf{u}} = (M_b\hat{p})^2 - (\mathbf{n}\cdot\hat{\mathbf{u}})^2 + \hat{\mathbf{u}}\cdot\hat{\mathbf{u}}. \tag{42}$$

At this point, one may substitute Eq. (42) into Eq. (38) and carry out the time averaging operation. This leaves

$$\alpha_6 = \frac{1}{4}E_m^{-2}\iint_{S_b} M_b(M_b^2\{1-[A_b^{(r)}]^2\}\hat{p}^2 + \hat{\mathbf{u}}_m\cdot\hat{\mathbf{u}}_m)\,\mathrm{d}S = \frac{1}{4}E_m^{-2}\iint_{S_b} M_b(\hat{\mathbf{u}}_m\cdot\hat{\mathbf{u}}_m)\,\mathrm{d}S + O(M_b^3). \tag{43}$$

Then using $\hat{\mathbf{u}}_m = -\nabla\hat{p}_m/k_m$, Eq. (43) becomes

$$\alpha_6 = \frac{1}{4}k_m^{-2}E_m^{-2}\iint_{S_b} M_b(\nabla\hat{p}_m)^2\,\mathrm{d}S. \tag{44}$$

Evaluation for the simple test motor gives

$$\alpha_6 = \tfrac{2}{5}M_b. \tag{45}$$

2.2.7. Viscous integral

The next two rotational groups in Eq. (1) involve viscous damping expressions. For example, a correction to the dilatational effect is represented in the seventh rotational term which may be transformed into a surface integral using

$$\frac{4}{3}\iiint_V \langle\delta^2\tilde{\mathbf{u}}\cdot\nabla(\nabla\cdot\hat{\mathbf{u}})\rangle\,\mathrm{d}V = -\frac{4}{3}\delta^2\iint_S \langle\mathbf{n}\cdot\tilde{\mathbf{u}}\partial\hat{p}/\partial t\rangle\,\mathrm{d}S. \tag{46}$$

Clearly, Eq. (46) must be negligible insofar as it scales with the product of δ^2 and the radial unsteady velocity at the boundaries. Contrarily, the eighth term with viscous damping is not small; it leads to

$$\alpha_7 = E_m^{-2}\exp(-2\alpha_m t)\iiint_V \langle-\delta^2(\hat{\mathbf{u}}+\tilde{\mathbf{u}})\cdot(\nabla\times\boldsymbol{\omega})\rangle\,\mathrm{d}V. \tag{47}$$

Then using $\mathbf{u}^{(1)} = \hat{\mathbf{u}} + \tilde{\mathbf{u}}$, one can put

$$\alpha_7 = -\delta^2 E_m^{-2}\exp(-2\alpha_m t)\iiint_V \langle\mathbf{u}^{(1)}\cdot(\nabla\times\boldsymbol{\omega})\rangle\,\mathrm{d}V. \tag{48}$$

Given that the conversion of α_7 constitutes a problem in its own right, its analysis is summarized in Appendix B. Its main result is

$$\alpha_7 = -\frac{1}{2}\delta^2 E_m^{-2}\exp(-2\alpha_m t)\left(\frac{k_m}{M_b}\right)^2\iint_S \langle\tilde{u}^2\rangle\Big|_{r=1}\,\mathrm{d}S. \tag{49}$$

To satisfy no slip at the surface, one puts $\tilde{u}_m = -\hat{u}_m$. Recalling that $\hat{u}_m = \sin(k_m z)$ for a longitudinal plane wave, one is left with

$$\alpha_7 = -\frac{1}{4}\delta^2 E_m^{-2}(k_m/M_b)^2\iint_S [\sin^2(k_m z)]\,\mathrm{d}S, \tag{50}$$

or, equivalently,

$$\alpha_7 = -\frac{1}{4}\delta^2 E_m^{-2}M_b^{-2}\iint_S \left(\frac{\partial\hat{p}_m}{\partial z}\right)^2\mathrm{d}S. \tag{51}$$

For a chamber dominated by longitudinal waves, one gets

$$\alpha_7 = -\frac{1}{4}\delta^2 E_m^{-2} M_b^{-2} \iint_S \left(\frac{\partial \hat{p}_m}{\partial z}\right)^2 \mathrm{d}S \approx -\frac{4}{15}\xi M_b, \tag{52}$$

where the approximation corresponds to the internal burning cylinder.

2.2.8. Pseudo acoustical integral

The pseudo acoustical correction is due to the relatively small pseudopressure that accompanies the vortical field and its coupling with either the unsteady acoustical or rotational velocities. It has been shown that this term is negligible, being $O(M_b{}^3)$ [33,43]. The first of these two terms can be expressed as

$$\alpha_8 = E_m^{-2} \exp(-2\alpha_m t) \iiint_V \langle -\hat{\mathbf{u}} \cdot \nabla \tilde{p} \rangle \, \mathrm{d}V. \tag{53}$$

A step-by-step derivation of the asymptotic closed-form solution for an internal burning cylinder is given by Majdalani et al. [33], specifically,

$$\alpha_8 = \frac{2M_b^3 l^2}{5m^2}\left[1 - 3\xi^2 \frac{M_b^2 l^2}{(m\pi)^2}\right] \ll O(1). \tag{54}$$

Despite the applicability of Eq. (54) to circular-port chambers, its small order of magnitude is typical of that calculated for other motors. It appears that this particular pseudo acoustical contribution remains small regardless of the motor shape [30].

2.2.9. Pseudo rotational integral

The next growth rate factor is due to the less obvious coupling that is formed between vorticity-induced pseudopressure and the unsteady rotational velocity. The significance of this term may be captured by examining

$$\alpha_9 = -E_m^{-2} \exp(-2\alpha_m t) \iiint_V \langle \tilde{\mathbf{u}} \cdot \nabla \tilde{p} \rangle \, \mathrm{d}V. \tag{55}$$

By use of vector identities, one can put

$$\alpha_9 = -E_m^{-2} \exp(-2\alpha_m t) \iiint_V \langle \nabla \cdot (\tilde{\mathbf{u}}\tilde{p}) \rangle \, \mathrm{d}V. \tag{56}$$

Subsequently, application of the divergence theorem yields

$$\alpha_9 = -E_m^{-2} \exp(-2\alpha_m t) \iint_S \langle \mathbf{n} \cdot (\tilde{\mathbf{u}}\tilde{p}) \rangle \, \mathrm{d}S. \tag{57}$$

The angle brackets may be removed through time averaging, thus changing Eq. (57) into

$$\alpha_9 = -\frac{1}{2} E_m^{-2} \iint_{S_N} (\tilde{u}_m^r \tilde{p}_m^r + \tilde{u}_m^i \tilde{p}_m^i) \, \mathrm{d}S. \tag{58}$$

Unlike α_8, this term can be expanded for two simple geometric shapes (slab and circular-port motors) and shown to be large. In the case of a circular-port motor, α_9 can be asymptotically expanded into [33]

$$\begin{aligned} \alpha_9 &= \tfrac{9}{200}\pi^2 l M_b E_m^{-2}[(\xi^2 - \tfrac{3}{2}) \exp(-2\xi) + \tfrac{3}{2} - 3\xi + 2\xi^2]\xi^{-4} \\ &\simeq \tfrac{9}{200}\pi^2 l M_b E_m^{-2}(1 - \tfrac{14}{15}\xi + \tfrac{8}{15}\xi^2 - \tfrac{8}{35}\xi^3 + \tfrac{5}{63}\xi^4 + \cdots). \end{aligned} \tag{59}$$

2.2.10. Unsteady nozzle integral

The 10th factor is the unsteady nozzle correction. It was shown previously that retention of unsteady rotational energy gives rise to a term at the downstream chamber boundary [33]. This growth rate combines the third and fourth rotational terms in Eq. (1) such that

$$\alpha_{10} = -M_b E_m^{-2} \exp(-2\alpha_m t) \iiint_V \langle (\hat{\mathbf{u}} + \tilde{\mathbf{u}}) \cdot \nabla (\mathbf{U} \cdot \tilde{\mathbf{u}}) \rangle \, \mathrm{d}V. \tag{60}$$

To convert Eq. (60) to a double integral, we first let $\mathbf{u}^{(1)} = \hat{\mathbf{u}} + \tilde{\mathbf{u}}$; the integrand unfolds into

$$\mathbf{u}^{(1)} \cdot [\nabla (\mathbf{U} \cdot \tilde{\mathbf{u}})] = \nabla \cdot [\mathbf{u}^{(1)} (\mathbf{U} \cdot \tilde{\mathbf{u}})] - (\mathbf{U} \cdot \tilde{\mathbf{u}}) \nabla \cdot \mathbf{u}^{(1)}. \tag{61}$$

The first term on the right-hand-side can then be replaced by

$$\iiint_V \langle \nabla \cdot [\mathbf{u}^{(1)} (\mathbf{U} \cdot \tilde{\mathbf{u}})] \rangle \, \mathrm{d}V = \iiint_V \langle \nabla \cdot [\tilde{\mathbf{u}} (\mathbf{U} \cdot \tilde{\mathbf{u}})] + \nabla \cdot [\hat{\mathbf{u}} (\mathbf{U} \cdot \tilde{\mathbf{u}})] \rangle \, \mathrm{d}V. \tag{62}$$

These integrals can be easily converted to surface form using the divergence theorem. For example, one can put

$$\iiint_V \langle \nabla \cdot [\tilde{\mathbf{u}} (\mathbf{U} \cdot \tilde{\mathbf{u}})] + \nabla \cdot [\hat{\mathbf{u}} (\mathbf{U} \cdot \tilde{\mathbf{u}})] \rangle \, \mathrm{d}V = \iint_S \langle \mathbf{n} \cdot [\tilde{\mathbf{u}} (\mathbf{U} \cdot \tilde{\mathbf{u}})] + \mathbf{n} \cdot [\hat{\mathbf{u}} (\mathbf{U} \cdot \tilde{\mathbf{u}})] \rangle \, \mathrm{d}S. \tag{63}$$

The normal projections of $\hat{\mathbf{u}}$ are $O(M_b)$; the second surface integral on the right-hand-side of Eq. (63) may be ignored, being $O(M^2{}_b)$. This turns Eq. (63) into

$$\iiint_V \langle \nabla \cdot [\tilde{\mathbf{u}} (\mathbf{U} \cdot \tilde{\mathbf{u}})] \rangle \, \mathrm{d}V = \iint_S \langle \mathbf{n} \cdot [\tilde{\mathbf{u}} (\mathbf{U} \cdot \tilde{\mathbf{u}})] \rangle \, \mathrm{d}S. \tag{64}$$

In like manner, the second term on the right-hand-side of Eq. (61) can be written as

$$-(\mathbf{U} \cdot \tilde{\mathbf{u}}) \nabla \cdot \mathbf{u}^{(1)} = -(\mathbf{U} \cdot \tilde{\mathbf{u}}) \nabla \cdot \hat{\mathbf{u}} - (\mathbf{U} \cdot \tilde{\mathbf{u}}) \nabla \cdot \tilde{\mathbf{u}}. \tag{65}$$

Since $\nabla \cdot \tilde{\mathbf{u}} = 0$, Eq. (65) simplifies into

$$(\mathbf{U} \cdot \tilde{\mathbf{u}}) \nabla \cdot \mathbf{u}^{(1)} = (\mathbf{U} \cdot \tilde{\mathbf{u}}) \nabla \cdot \hat{\mathbf{u}}. \tag{66}$$

At length, α_{10} becomes

$$\alpha_{10} = -M_b E_m^{-2} \exp(-2\alpha_m t) \left\{ \iint_S \langle \mathbf{n} \cdot [\tilde{\mathbf{u}} (\mathbf{U} \cdot \tilde{\mathbf{u}})] \rangle \, \mathrm{d}S - \iiint_V \langle (\mathbf{U} \cdot \tilde{\mathbf{u}}) \nabla \cdot \hat{\mathbf{u}} \rangle \, \mathrm{d}V \right\}. \tag{67}$$

Thus, by evaluating the second term on the right-hand-side of Eq. (67), one retrieves

$$\begin{aligned} \iiint_V \langle (\mathbf{U} \cdot \tilde{\mathbf{u}}) \nabla \cdot \hat{\mathbf{u}} \rangle \, \mathrm{d}V = \iiint_V \langle & k_m \pi z \cos(x) \sin(x) \mathrm{e}^{\phi} \sin(\psi) \sin[\sin(x) k_m z] \\ & \times \cos(k_m z) \mathrm{e}^{2\alpha_m t} \cos(k_m t) \sin(k_m t) \, \mathrm{d}V \rangle. \end{aligned} \tag{68}$$

As expected, the radial integral yields a value of $O(M_b)$. Although Eq. (68) corresponds to the case of a full-length circular-port motor, it may be shown that this component is small for other geometric shapes. For the general case of an arbitrary motor, one must evaluate

$$\alpha_{10} = -M_b E_m^{-2} \exp(-2\alpha_m t) \iint_S \langle \mathbf{n} \cdot [\tilde{\mathbf{u}} (\mathbf{U} \cdot \tilde{\mathbf{u}})] \rangle \, \mathrm{d}S. \tag{69}$$

Table 1
Rotational integrals in both volume and surface integral forms.

	Volume form	Surface form	SSP[a] form
$E_m^{\ 2}$	$E_m^2 = \frac{1}{2}\iiint_V [(\hat{p}_m)^2 + \hat{\mathbf{u}}_m \cdot \hat{\mathbf{u}}_m + 2\hat{\mathbf{u}}_m \cdot \tilde{\mathbf{u}}_m^i + \tilde{\mathbf{u}}_m^r \cdot \tilde{\mathbf{u}}_m^r + \tilde{\mathbf{u}}_m^i \cdot \tilde{\mathbf{u}}_m^i]\,\mathrm{d}V$		
α_1	$\frac{E_m^{-2}}{\exp(2\alpha_m t)}\iiint_V \left\langle -\nabla\cdot\left[\hat{p}\hat{\mathbf{u}} + \frac{1}{2}M_b\mathbf{U}(\hat{p})^2\right] - M_b[\hat{\mathbf{u}}\cdot\nabla(\mathbf{U}\cdot\hat{\mathbf{u}})]\right\rangle \mathrm{d}V$	$\frac{-E_m^{-2}}{\exp(2\alpha_m t)}\iint_S \left\langle \mathbf{n}\cdot\left[\hat{p}\hat{\mathbf{u}} + \frac{1}{2}M_b\mathbf{U}(\hat{p})^2\right] - M_b[\mathbf{n}\cdot\hat{\mathbf{u}}(\mathbf{U}\cdot\hat{\mathbf{u}})]\right\rangle \mathrm{d}S$	$\frac{1}{2}M_b E_m^{-2}\left\{\iint_{S_b}\hat{p}_m^2[A_b^{(r)}+1]\,\mathrm{d}S - \iint_{S_N}\hat{p}_m^2[A_N^{(r)}+U_N]\,\mathrm{d}S\right\}$
α_2	$\frac{E_m^{-2}}{\exp(2\alpha_m t)}\iiint_V \left\langle \frac{4}{3}\delta^2\hat{\mathbf{u}}\cdot\nabla(\nabla\cdot\hat{\mathbf{u}})\right\rangle \mathrm{d}V$	$\frac{4k_m\delta^2E_m^{-2}}{3\,\exp(2\alpha_m t)}\iint_S\langle\mathbf{n}\cdot(\hat{p}\hat{\mathbf{u}})\rangle\,\mathrm{d}S - \frac{1}{3}\delta^2E_m^{-2}k_m^2\pi l$	$-\frac{2}{3}k_m\delta^2E_m^{-2}\left[\iint_{S_b}M_bA_b^{(r)}\hat{p}_m^2\,\mathrm{d}S - \iint_{S_N}M_bA_N^{(r)}\hat{p}_m^2\,\mathrm{d}S + \frac{1}{2}k_m\pi l\right]$
α_3	$\frac{E_m^{-2}}{\exp(2\alpha_m t)}\iiint_V \langle M_b\{\hat{\mathbf{u}}\cdot(\hat{\mathbf{u}}\times\boldsymbol{\Omega})\}\rangle\,\mathrm{d}V$	0	0
α_4	$\frac{E_m^{-2}}{\exp(2\alpha_m t)}\iiint_V \langle M_b\hat{\mathbf{u}}\cdot(\mathbf{U}\times\boldsymbol{\omega})\rangle\,\mathrm{d}V$	$\frac{M_bE_m^{-2}}{\exp(\alpha_m t)}\iint_{S_b}\langle\tilde{\mathbf{u}}^i\cdot\hat{\mathbf{u}}\rangle\,\mathrm{d}S$	$-\frac{1}{2}M_bE_m^{-2}\iint_{S_b}\hat{\mathbf{u}}_m\cdot\hat{\mathbf{u}}_m\,\mathrm{d}S$
α_5	$\frac{E_m^{-2}}{\exp(2\alpha_m t)}\iiint_V \langle -\tilde{\mathbf{u}}\cdot\nabla\hat{p}\rangle\,\mathrm{d}V$	$\frac{-E_m^{-2}}{\exp(2\alpha_m t)}\iint_S\langle\mathbf{n}\cdot(\tilde{\mathbf{u}}\hat{p})\rangle\,\mathrm{d}S$	$\frac{1}{2}M_bE_m^{-2}\iint_{S_b}\hat{p}_m^2\,\mathrm{d}S$
α_6	$\frac{E_m^{-2}}{\exp(2\alpha_m t)}\iiint_V \langle M_b\tilde{\mathbf{u}}\cdot(\mathbf{U}\times\boldsymbol{\omega})\rangle\,\mathrm{d}V$	$\frac{-M_bE_m^{-2}}{\exp(2\alpha_m t)}\iint_S\left\langle\mathbf{n}\cdot\mathbf{U}\left(\frac{1}{2}\tilde{\mathbf{u}}\cdot\tilde{\mathbf{u}}\right)\right\rangle\mathrm{d}S$	$\frac{1}{4}k_m^{-2}M_bE_m^{-2}\iint_{S_b}(\nabla\hat{p}_m)^2\,\mathrm{d}S$
α_7	$\frac{E_m^{-2}}{\exp(2\alpha_m t)}\iiint_V \langle -\delta^2(\hat{\mathbf{u}}+\tilde{\mathbf{u}})\cdot(\nabla\times\boldsymbol{\omega})\rangle\,\mathrm{d}V$	$-\frac{\delta^2E_m^{-2}k_m^2M_b^{-2}}{2\,\exp(2\alpha_m t)}\iint_S\langle\tilde{\mathbf{u}}^2\rangle\Big\vert_{r=1}\mathrm{d}S$	$-\frac{1}{4}\delta^2E_m^{-2}M_b^{-2}\iint_{S_b}(\nabla\hat{p}_m)^2\,\mathrm{d}S$
α_8	$\frac{E_m^{-2}}{\exp(2\alpha_m t)}\iiint_V \langle -\hat{\mathbf{u}}\cdot\nabla\tilde{p}\rangle\,\mathrm{d}V$	$\frac{2M_b^3l^2}{5m^2}$	$\frac{2M_b^3l^2}{5m^2}$
α_9	$\frac{-E_m^{-2}}{\exp(2\alpha_m t)}\iiint_V \langle\tilde{\mathbf{u}}\cdot\nabla\tilde{p}\rangle\,\mathrm{d}V$	$\frac{-E_m^{-2}}{\exp(2\alpha_m t)}\iint_S\langle\mathbf{n}\cdot\tilde{\mathbf{u}}\tilde{p}\rangle\,\mathrm{d}S$	$\frac{-1}{2}E_m^{-2}\iint_{S_N}[\tilde{u}_m^r\tilde{p}_m^r + \tilde{u}_m^i\tilde{p}_m^i]\,\mathrm{d}S$
α_{10}	$\frac{-E_m^{-2}}{\exp(2\alpha_m t)}\iiint_V \langle M_b(\hat{\mathbf{u}}+\tilde{\mathbf{u}})\cdot\nabla(\mathbf{U}\cdot\tilde{\mathbf{u}})\rangle\,\mathrm{d}V$	$\frac{-M_bE_m^{-2}}{\exp(2\alpha_m t)}\iint_S\langle\hat{\mathbf{n}}\cdot[\tilde{\mathbf{u}}(\mathbf{U}\cdot\tilde{\mathbf{u}})]\rangle\,\mathrm{d}S$	$\frac{-M_b}{2E_m^2}\iint_{S_N}[(\tilde{u}_m^i)^2 + (\tilde{u}_m^r)^2]U_z\,\mathrm{d}S$

[a]Standard stability prediction code used by French et al. [22].

Finally, time averaging of Eq. (69) turns it into

$$\alpha_{10} = -\frac{1}{2} M_b E_m^{-2} \iint_{S_N} [(\tilde{u}_m^r)^2 + (\tilde{u}_m^i)^2] U_z \, \mathrm{d}S. \tag{70}$$

For the circular-port motor geometry, α_{10} may be asymptotically approximated [33]. Its small ξ expansion renders

$$\begin{aligned} \alpha_{10} &= -\tfrac{9}{200}\pi^2 l M_b E_m^{-2}[(\xi^2 - \tfrac{3}{2})\exp(-2\xi) + \tfrac{3}{2} - 3\xi + 2\xi^2]\xi^{-4} \\ &\simeq -\tfrac{9}{200}\pi^2 l M_b E_m^{-2}(1 - \tfrac{14}{15}\xi + \tfrac{8}{15}\xi^2 - \tfrac{8}{35}\xi^3 + \tfrac{5}{63}\xi^4 + \cdots). \end{aligned} \tag{71}$$

In the interest of clarity, the 10 converted integrals are summarized in Table 1.

3. Results and discussion

3.1. Verification

Numerical integration of the surface integrals was performed for a group of representative chamber lengths and grains. Three routinely used cases were selected as characteristic examples for testing the present formulation [43]. These representative motors were chosen because they aptly characterize a wide range of motors. Table 2 lists their physical and geometric parameters. The dimensional growth rates for the representative motors are calculated and posted in Table 3. The growth rates are normalized using $\alpha^* = \alpha a_0/R$, where the asterisk (*) denotes a dimensional quantity. The acoustic mean flow correction, $\alpha_3 = 0$, is omitted. It may be instructive to note that a similar numerical study has been performed [33] in which the original volume integrals were evaluated for a circular-port motor and the same three cases delineated in Table 2. Results of those volume integrals can be compared to the ones obtained here in an effort to validate the surface formulation. To this end, the outcome derived from volume integration is displayed in Table 3, thus illustrating the level of agreement between the two methods. One major advantage of the surface form stands in its sole dependence on the acoustic field.

Table 2
Physical parameters for the routinely cited representative cases [43].

Motor	L (m)	R (m)	M_b	δ	k_m	S	ξ	f (Hz)	$A_b^{(r)}$	(m/s)
Small motor	0.60	0.025	1.7^{-3}	5.49^{-4}	1.31^{-1}	77.00	1.0512	1227	2.5	1472
Tactical rocket	2.03	0.102	3.1^{-3}	2.74^{-4}	1.58^{-1}	50.92	0.0628	360	1.2	1462
RSRM	35.1	0.700	2.3^{-3}	1.04^{-4}	6.27^{-2}	27.24	0.0035	19.5	1.0	1369

Table 3
Numerically evaluated integrals of individual growth rates (s^{-1}) [33].

Motor	Study	α_1^*	α_2^*	α_4^*	α_5^*	α_6^*	α_7^*	α_8^*	α_9^*	α_{10}^*
Small motor	Surface	96.1	-1.62^{-4}	−80.1	80.1	40.0	−28.06	0.0644	11.5	−11.5
	Volume	96.1	-1.62^{-4}	−80.0	80.0	39.2	−18.61	0.0644	11.5	−11.5
Tactical rocket	Surface	−3.55	-1.43^{-5}	−35.5	35.5	17.8	−0.744	0.0627	9.62	−9.62
	Volume	−3.55	-1.43^{-5}	−35.7	35.7	16.5	−0.716	0.0627	9.62	−9.62
RSRM	Surface	−1.08	-4.43^{-8}	−3.60	3.60	1.80	−0.00419	0.0179	1.01	−1.01
	Volume	−1.08	-4.43^{-8}	−3.66	3.66	1.66	−0.00411	0.0179	1.01	−1.01

Table 4
SSP evaluated surface integrals of individual growth rates (s^{-1}).

Motor	α_1^*	α_4^*	α_5^*	α_6^*	α_7^*
Small motor	96.41	−80.01	80.01	40.04	−28.03
Tactical rocket	−3.52	−35.54	35.54	17.78	−0.744
Space shuttle SRB	−1.08	−3.60	3.60	1.80	−0.0042

One point of discrepancy in Table 3 stems from the evaluation of the viscous correction, α_7, for the small motor (where an error of 33 percent is accrued). This relatively large error can be attributed to the small motor having a viscous parameter in excess of unity. By virtue of the asymptotic approximations used in the derivation process, the range of applicability for the closed-form solutions must be bracketed, specifically to motors with $\xi < 1$. This requirement is not too restrictive, as most practical motors are characterized by a small viscous parameter.

The other eight growth rate integrals display a maximum error of 8.4 percent; this peak error occurs in α_6 for the reusable solid rocket motor (RSRM). The overall level of agreement between volume and surface integrals is showcased in Table 3; it may be deemed satisfactory in most engineering applications, especially when considering the uncertainties associated with the acquisition of combustion instability data. While flow variables can be difficult to calculate throughout the chamber, the new surface forms mitigate this problem by providing integrals that are more easily amenable to evaluation.

Before leaving this subject, we insist that numerical evaluation of the surface integrals be performed independently, using the standard stability prediction code. This code makes use of the growth rate factors that are of $O(M_b)$ and larger. As such, α_2, α_3 and α_8 are not calculated. In Table 4, separately acquired results are presented to allow for their comparison to ours. Clearly, the new computations are found to be in excellent agreement with the numerically evaluated integrals of Table 3.

3.2. Discussion

The transformed integrals are collected in Table 1 where the original and newly converted forms are listed side-by-side. The surface integrals are expressed in field vector form, before time averaging, and also in a form that is most suitable for implementation in acoustical codes. It must be noted that these integrals correspond to the linear growth rate behaviour preceding the onset of nonlinear oscillations. A similar analysis needs to be applied to the nonlinear growth rate integrals that control the system behaviour during wave steepening and establishment of limit cycle amplitudes.

Of the 10 integrals posted in Table 1, it should be noted that only seven are important. These include (i) pressure coupling α_1, (ii) flow turning α_4, (iii) rotational flow correction α_5, (iv) mean vortical correction α_6, (v) viscous damping α_7, (vi) pseudo rotational correction α_9, and (vii) unsteady nozzle correction α_{10}. Two important corrections not covered here are due to particle damping and distributed combustion. These are covered quite thoroughly by Culick and Yang [51].

Having obtained the surface integral forms of the most significant growth rate contributions, the newly simplified expressions may be readily incorporated into numerical codes as reported in Ref. [22].

Another key aspect that this study addresses is the impact of retaining the pseudopressure. Being the unsteady pressure wave (or pseudosound) generated at solid boundaries, $\tilde{p}$ is ignored in most stability calculations because of (a) its small magnitude and (b) its rapid decay away from the burning surface. However, considering that most important stability interactions occur in the vicinity of the propellant surface, it is not surprising that one of the two pseudo corrections is not negligible (i.e., α_9). This point is confirmed in the present analysis as pseudo-related corrections are examined in both volume and surface form. Interestingly, α_9 and α_{10} are self-cancelling despite their widely dissimilar acoustic sources (α_{10} is due to unsteady energy exiting the chamber).

4. Closing remarks

This study showcases a step forward in improving the mathematical modelling of acoustic energy for chambers undergoing linear oscillations. Its usefulness lies in the simplification of the growth rate expressions to equivalent, albeit more manageable identities and approximations. The converted surface integrals are obtained in conceptual form that is independent of chamber geometry, although the validation is carried out for the case of a circular-port chamber. Based on three representative motors, the newly derived surface integral representations of the combustion instability growth rate factors may be substituted for the more complex volume forms. It must be remembered that the surface integrals assume small viscosity ($\xi<1$) and correspond to the linear growth rate behaviour preceding the onset of nonlinear oscillations. So while our stability integrals remain general, our evaluation of these integrals is limited to the test case considered here, namely, to that of an internal burning cylindrical motor. When more complex geometric shapes are considered, one must obtain the mode shapes and frequencies numerically.

Acknowledgements

This project is sponsored partly by the National Science Foundation (Grant no. CMMI-0353518) and partly by the University of Tennessee Space Institute through institutional cost sharing.

Appendix A. Vortical correction

This section delineates the procedure for converting α_6. This factor is dubbed the mean vortical correction and consists of

$$\alpha_6 = E_m^{-2}\exp(-2\alpha_m t)\iiint_V \langle M_b\tilde{\mathbf{u}}\cdot(\mathbf{U}\times\boldsymbol{\omega})\rangle\,\mathrm{d}V. \tag{A.1}$$

Eq. (A.1) can be further simplified using $\boldsymbol{\omega}=\nabla\times\tilde{\mathbf{u}}$, namely,

$$\alpha_6 = M_b E_m^{-2}\exp(-2\alpha_m t)\iiint_V \langle\tilde{\mathbf{u}}\cdot[\mathbf{U}\times(\nabla\times\tilde{\mathbf{u}})]\rangle\,\mathrm{d}V. \tag{A.2}$$

Upon expansion, one finds

$$\nabla\times\tilde{\mathbf{u}} = \left(\frac{\partial\tilde{u}_r}{\partial z}-\frac{\partial\tilde{u}_z}{\partial r}\right)\hat{\mathbf{e}}_\theta. \tag{A.3}$$

Note that Eq. (A.3) is contingent upon the unsteady rotational velocity being axisymmetric and having no θ-component. The integrand becomes

$$\tilde{\mathbf{u}}\cdot[\mathbf{U}\times(\nabla\times\tilde{\mathbf{u}})] = -\tilde{u}_r U_z\left(\frac{\partial\tilde{u}_r}{\partial z}-\frac{\partial\tilde{u}_z}{\partial r}\right)+\tilde{u}_z U_r\left(\frac{\partial\tilde{u}_r}{\partial z}-\frac{\partial\tilde{u}_z}{\partial r}\right). \tag{A.4}$$

Recalling that $\partial\tilde{u}_r/\partial z = O(M_b^2)$, one is left with

$$\tilde{\mathbf{u}}\cdot[\mathbf{U}\times(\nabla\times\tilde{\mathbf{u}})] = \tilde{u}_r U_z\frac{\partial\tilde{u}_z}{\partial r}-\tilde{u}_z U_r\frac{\partial\tilde{u}_z}{\partial r}. \tag{A.5}$$

The first term on the right-hand-side of Eq. (A.5) can be shown to be negligible. Considering that $\tilde{u}_r = O(M_b)$, this term combines with the M_b on the outside of the volume integral to yield $O(M_b^2)$. Consequently, Eq. (A.5) becomes

$$\tilde{\mathbf{u}}\cdot[\mathbf{U}\times(\nabla\times\tilde{\mathbf{u}})] = -\tilde{u}_z U_r\frac{\partial\tilde{u}_z}{\partial r}. \tag{A.6}$$

At this juncture, we may shift our attention to the term

$$\nabla\cdot(\mathbf{U}\tfrac{1}{2}\tilde{\mathbf{u}}\cdot\tilde{\mathbf{u}}) = \tfrac{1}{2}\nabla\cdot[\mathbf{U}(\tilde{u}_r\tilde{u}_r+\tilde{u}_z\tilde{u}_z)]. \tag{A.7}$$

Recalling that $\nabla \cdot \mathbf{U} = 0$, it is straightforward to show that Eq. (A.7) may be expanded and simplified into

$$\nabla \cdot \left[\mathbf{U} \left(\frac{1}{2} \tilde{\mathbf{u}} \cdot \tilde{\mathbf{u}} \right) \right] = U_r \tilde{u}_r \frac{\partial \tilde{u}_r}{\partial r} + U_z \tilde{u}_r \frac{\partial \tilde{u}_r}{\partial z} + U_z \tilde{u}_z \frac{\partial \tilde{u}_z}{\partial z} + U_r \tilde{u}_z \frac{\partial \tilde{u}_z}{\partial r}. \tag{A.8}$$

Then, owing to $\partial \tilde{u}_r / \partial z = O(M_b^2)$, Eq. (A.8) reduces to

$$\nabla \cdot \left[\mathbf{U} \left(\frac{1}{2} \tilde{\mathbf{u}} \cdot \tilde{\mathbf{u}} \right) \right] = U_r \tilde{u}_r \frac{\partial \tilde{u}_r}{\partial r} + U_z \tilde{u}_z \frac{\partial \tilde{u}_z}{\partial z} + U_r \tilde{u}_z \frac{\partial \tilde{u}_z}{\partial r}. \tag{A.9}$$

The first term on the right-hand-side of Eq. (A.9) is also small because $\tilde{u}_r = O(M_b)$; one is left with

$$\nabla \cdot \left[\mathbf{U} \left(\frac{1}{2} \tilde{\mathbf{u}} \cdot \tilde{\mathbf{u}} \right) \right] = U_z \tilde{u}_z \frac{\partial \tilde{u}_z}{\partial z} + U_r \tilde{u}_z \frac{\partial \tilde{u}_z}{\partial r}. \tag{A.10}$$

Forthwith, the integral of the first term on the right-hand-side of Eq. (A.10) yields

$$\begin{aligned} \mathrm{I} = \iiint_V \left\langle U_z \tilde{u}_z \frac{\partial \tilde{u}_z}{\partial z} \right\rangle \mathrm{d}V = \iiint_V \Bigg\langle & \pi z \cos(x) \, \mathrm{e}^{2\alpha_m t} [\tilde{u}_m^r \cos(k_m t) + \tilde{u}_m^i \sin(k_m t)] \\ & \times \left[\frac{\partial \tilde{u}_m^r}{\partial z} \cos(k_m t) + \frac{\partial \tilde{u}_m^i}{\partial z} \sin(k_m t) \right] \Bigg\rangle \mathrm{d}V. \end{aligned} \tag{A.11}$$

Then, through time averaging, one collects

$$\mathrm{I} = \iiint_V \tfrac{1}{2} \pi z \cos(x) \, \mathrm{e}^{2\alpha_m t} \left(\tilde{u}_m^r \frac{\partial \tilde{u}_m^r}{\partial z} + \tilde{u}_m^i \frac{\partial \tilde{u}_m^i}{\partial z} \right) \mathrm{d}V. \tag{A.12}$$

Additionally, substituting the expressions for $\tilde{u}_m^r$ and $\tilde{u}_m^i$ renders

$$\begin{aligned} \mathrm{I} = & \frac{1}{2} k_m \pi \, \mathrm{e}^{2\alpha_m t} \iiint_V z \cos(x) \sin^3(x) \, \mathrm{e}^{2\phi} \sin[\sin(x) k_m z] \\ & \times \{ \sin^2(\psi) \cos[\sin(x) k_m z] + \cos^2(\psi) \cos[\sin(x) k_m z] \} \, \mathrm{d}V. \end{aligned} \tag{A.13}$$

As shown before [37], the phase angle $\psi(r) = -[k_m/(\pi M_b)] \ln \tan(\frac{1}{2}x)$ controls the wavelength and spatial frequency of rotational shear waves. The real argument, $\phi(r)$, is responsible for viscous damping. Hence, one may put

$$\mathrm{I} = \frac{1}{2} k_m \pi \, \mathrm{e}^{2\alpha_m t} \int_0^l \int_0^{2\pi} \int_0^1 z \cos(x) \sin^3(x) \, \mathrm{e}^{2\phi} \sin[\sin(x) k_m z] \cos[\sin(x) k_m z] r \, \mathrm{d}r \, \mathrm{d}\theta \, \mathrm{d}z. \tag{A.14}$$

It can be shown that this part is negligible, being of $O(M_b{}^2)$. Eq. (A.10) reduces to

$$-\nabla \cdot \mathbf{U} \left(\frac{1}{2} \tilde{\mathbf{u}} \cdot \tilde{\mathbf{u}} \right) = -U_r \tilde{u}_z \frac{\partial \tilde{u}_z}{\partial r}. \tag{A.15}$$

Note that Eq. (A.6) may be replaced by Eq. (A.15). Then using the divergence theorem, one retrieves

$$\alpha_6 = \frac{-M_b E_m^{-2}}{\exp(2\alpha_m t)} \iint_S \left\langle \mathbf{n} \cdot \left[\mathbf{U} \left(\frac{1}{2} \tilde{\mathbf{u}} \cdot \tilde{\mathbf{u}} \right) \right] \right\rangle \mathrm{d}S. \tag{A.16}$$

Appendix B. Viscous correction

This Appendix delineates the main procedure for converting α_7 given

$$\alpha_7 = -\delta^2 E_m^{-2} \exp(-2\alpha_m t) \iiint_V \langle \mathbf{u}^{(1)} \cdot (\nabla \times \boldsymbol{\omega}) \rangle \, \mathrm{d}V. \tag{B.1}$$

Eq. (B.1) may be simplified by the use of the identity, $\nabla\cdot(\mathbf{A}\times\mathbf{B})=\mathbf{B}\cdot(\nabla\times\mathbf{A})-\mathbf{A}\cdot(\nabla\times\mathbf{B})$; this translates into

$$\mathbf{u}^{(1)}\cdot(\nabla\times\boldsymbol{\omega})=\nabla\cdot[\boldsymbol{\omega}\times\mathbf{u}^{(1)}]+\boldsymbol{\omega}\cdot[\nabla\times\mathbf{u}^{(1)}]. \tag{B.2}$$

Then, recalling that

$$\nabla\times\hat{\mathbf{u}}=0,\quad \nabla\times\tilde{\mathbf{u}}=\boldsymbol{\omega},\quad \nabla\times\mathbf{u}^{(1)}=\boldsymbol{\omega}, \tag{B.3}$$

one can put

$$\mathbf{u}^{(1)}\cdot(\nabla\times\boldsymbol{\omega})=\nabla\cdot[\boldsymbol{\omega}\times\mathbf{u}^{(1)}]+\boldsymbol{\omega}\cdot\boldsymbol{\omega}, \tag{B.4}$$

such that

$$\alpha_7=-\delta^2E_m^{-2}\exp(-2\alpha_m t)\iiint_V\langle\nabla\cdot[\boldsymbol{\omega}\times\mathbf{u}^{(1)}]+\boldsymbol{\omega}\cdot\boldsymbol{\omega}\rangle\,\mathrm{d}V. \tag{B.5}$$

This volume integral may be separated and partially converted to a surface integral using the divergence theorem. The first term in Eq. (B.5) yields

$$\iiint_V\langle\nabla\cdot[\boldsymbol{\omega}\times\mathbf{u}^{(1)}]\rangle\,\mathrm{d}V=\iint_S\langle\mathbf{n}\cdot[\boldsymbol{\omega}\times\mathbf{u}^{(1)}]\rangle\,\mathrm{d}S. \tag{B.6}$$

Fortuitously, this term simply vanishes. This is caused by the necessity of $\mathbf{u}^{(1)}$ to remain parallel to $\mathbf{n}$. In adherence to the no-slip requirement at the surface, there can be no velocity component parallel to the grain the surface. One is left with

$$\iiint_V\langle\mathbf{u}^{(1)}\cdot\nabla\times\boldsymbol{\omega}\rangle\,\mathrm{d}V=\iiint_V\langle\boldsymbol{\omega}\cdot\boldsymbol{\omega}\rangle\,\mathrm{d}V, \tag{B.7}$$

and so

$$\alpha_7=-\delta^2E_m^{-2}\exp(-2\alpha_m t)\iiint_V\langle\boldsymbol{\omega}\cdot\boldsymbol{\omega}\rangle\,\mathrm{d}V. \tag{B.8}$$

The resulting integrand is a scalar. The corresponding physical problem displays conventional boundary layer behaviour. One can therefore employ the Von Kàrmàn–Polhausen method and evaluate the part of the integral normal to the surface. At the wall,

$$\boldsymbol{\omega}=\nabla\times\mathbf{u}^{(1)}=\tilde{\omega}\mathbf{e}_\theta=\left(\frac{\partial\tilde{u}_r}{\partial z}-\frac{\partial\tilde{u}_z}{\partial r}\right)\mathbf{e}_\theta=-\frac{\partial\tilde{u}_z}{\partial r}\mathbf{e}_\theta, \tag{B.9}$$

where

$$\begin{cases}\tilde{u}_z=\mathrm{e}^{\alpha_m t}\sin(x)\exp(\phi)\sin[\sin(x)k_m z][\sin(\psi)\cos(k_m t)-\cos(\psi)\sin(k_m t)];\quad x=\dfrac{1}{2}\pi r^2,\\ \tilde{\omega}=\dfrac{k_m}{M_b}\mathrm{e}^{\alpha_m t}r\exp(\phi)\sin[\sin(x)k_m z][\cos(\psi)\cos(k_m t)+\sin(\psi)\sin(k_m t)]+O(1),\end{cases} \tag{B.10}$$

and so

$$\boldsymbol{\omega}\cdot\boldsymbol{\omega}=\left(\frac{k_m}{M_b}\right)^2\mathrm{e}^{2\alpha_m t}\{r\exp(\phi)\sin[k_m z\sin(x)]\}^2[\cos(\psi)\cos(k_m t)+\sin(\psi)\sin(k_m t)]^2. \tag{B.11}$$

In order to further simplify Eq. (B.11), time averaging may be applied. Given two dissimilar time scales for oscillations and wave attenuation, one obtains

$$\langle\boldsymbol{\omega}\cdot\boldsymbol{\omega}\rangle=\tfrac{1}{2}(k_m/M_b)^2\,\mathrm{e}^{2\alpha_m t}\{r\exp(\phi)\sin[k_m z\sin(x)]\}^2. \tag{B.12}$$

To make headway, it is instructive to digress and consider the unsteady rotational velocity. When time averaging is performed for $\tilde{u}_z^2$, one gets

$$\langle \tilde{u}_z^2 \rangle = \tfrac{1}{2} \mathrm{e}^{2\alpha_m t} \{\sin(x)\, \exp(\phi)\, \sin[k_m z\, \sin(x)]\}^2. \tag{B.13}$$

Noting that vorticity effects are most pronounced near the surface where $r = \sin(x) = 1$, one can put

$$\begin{cases} \langle \boldsymbol{\omega} \cdot \boldsymbol{\omega} \rangle \approx \tfrac{1}{2}(k_m/M_b)^2\, \mathrm{e}^{2\alpha_m t} \{\exp(\phi)\, \sin[k_m z\, \sin(x)]\}^2 \\ \langle \tilde{u}_z^2 \rangle \approx \tfrac{1}{2} \mathrm{e}^{2\alpha_m t} \{\exp(\phi)\, \sin[k_m z\, \sin(x)]\}^2 \end{cases} \tag{B.14}$$

Hence, to leading order approximation, one has

$$\langle \boldsymbol{\omega} \cdot \boldsymbol{\omega} \rangle \approx \left\langle \frac{1}{2} \left(\frac{k_m}{M_b} \right)^2 \frac{\partial \tilde{u}_z^2}{\partial r} \right\rangle. \tag{B.15}$$

At the outset, α_7 becomes

$$\alpha_7 = -\frac{1}{4} \delta^2 E_m^{-2} (k_m/M_b)^2 \iiint_V \frac{\partial \tilde{u}_m^2}{\partial r}\, \mathrm{d}V. \tag{B.16}$$

Thus, for the circular-port motor, one can write

$$\alpha_7 = -\frac{1}{4} \delta^2 E_m^{-2} (k_m/M_b)^2 \iint_S \left(\int_0^1 \frac{\partial \tilde{u}_m^2}{\partial r}\, \mathrm{d}r \right) \mathrm{d}S. \tag{B.17}$$

This expression reduces to

$$\alpha_7 = -\frac{1}{4} \delta^2 E_m^{-2} (k_m/M_b)^2 \iint_S \tilde{u}_m^2 \Big|_{r=1}\, \mathrm{d}S, \tag{B.18}$$

which corresponds to the non-time averaged form

$$\alpha_7 = -\frac{\delta^2 E_m^{-2}}{2\, \exp(2\alpha_m t)} \left(\frac{k_m}{M_b} \right)^2 \iint_S \langle \tilde{u}^2 \rangle \Big|_{r=1}\, \mathrm{d}S. \tag{B.19}$$

The accuracy of the above approximation increases as the Taylor–Culick mean flow is replaced by a more realistic turbulent profile. When turbulence prevails, damping of unsteady velocities and vorticity occurs more rapidly while their magnitudes near the wall remain the same (see Ref. [52]). Under such conditions, the velocity integral in the radial direction approaches its value at the injection surface.

References

[1] L. Crocco, S.I. Cheng, *Theory of Combustion Instability in Liquid Propellant Rocket Motors, AGARD*, Vol. 8, Butterworths Sci. Pub. Ltd., London, UK, 1956.

[2] L. Crocco, S.I. Cheng, High frequency combustion instability in rocket motors with concentrated combustion, *Journal of the American Rocket Society* 23 (1953) 301–313.

[3] W.A. Sirignano, L. Crocco, A shock wave model of unstable rocket combustion, *AIAA Journal* 2 (1964) 1285–1296.

[4] C. Mitchell, Axial Mode Shock Wave Combustion Instability in Liquid Propellant Rocket Engines, PhD Dissertation, Princeton University, 1967.

[5] B.T. Zinn, A theoretical study of nonlinear combustion instability in liquid propellant engines, *AIAA Journal* 6 (1968) 1966–1972.

[6] F.E.C. Culick, High frequency oscillations in liquid rockets, *AIAA Journal* 1 (1963) 1097–1104.

[7] G.A. Flandro, Solid propellant acoustic admittance corrections, *Journal of Sound and Vibration* 36 (1974) 297–312.

[8] G.A. Flandro, Effects of vorticity on rocket combustion stability, *Journal of Propulsion and Power* 11 (1995) 607–625.

[9] G.A. Flandro, Vortex driving mechanisms in oscillatory rocket flows, *Journal of Propulsion and Power* 2 (1986) 206–214.

[10] G.A. Flandro, Energy balance analysis of nonlinear combustion instability, *Journal of Propulsion and Power* 1 (1985) 210–221.

[11] R.W. Hart, F.T. McClure, Combustion instability: acoustic interaction with a burning propellant surface, *The Journal of Chemical Physics* 10 (1959) 1501–1514.
[12] R.W. Hart, F.T. McClure, Theory of acoustic instability in solid propellant rocket combustion, *10th Symposium* (*International*) *on Combustion*, 1964, pp. 1047–1066.
[13] F.S. Blomshield, H.B. Mathes, Pressure oscillations in post-Challenger space shuttle redesigned solid rocket motors, *Journal of Propulsion and Power* 9 (1993) 217–221.
[14] F.S. Blomshield, H.B. Mathes, J.E. Crump, C.A. Beiter, M.W. Beckstead, Nonlinear stability testing of full-scale tactical motors, *Journal of Propulsion and Power* 13 (1997) 356–366.
[15] F.S. Blomshield, J.E. Crump, H.B. Mathes, R.A. Stalnaker, M.W. Beckstead, Stability testing of full-scale tactical motors, *Journal of Propulsion and Power* 13 (1997) 349–355.
[16] Y. Fabignon, J. Dupays, G. Avalon, F. Vuillot, N. Lupoglazoff, G. Casalis, M. Prévost, Instabilities and pressure oscillations in solid rocket motors, *Journal of Aerospace Science and Technology* 7 (2003) 191–200.
[17] S. Apte, V. Yang, Effect of acoustic oscillation on flow development in a simulated nozzleless rocket motor, in: V. Yang, T.B. Brill, W.-Z. Ren (Eds.), *Solid Propellant Chemistry, Combustion, and Motor Interior Ballistics*, Vol. 185, AIAA Progress in Astronautics and Aeronautics, Washington, DC, 2000, pp. 791–822.
[18] T.S. Roh, S. Apte, V. Yang, Combustion dynamics of homogeneous solid propellants in a rocket motor with acoustic excitations, in: V. Yang, T.B. Brill, W.-Z. Ren (Eds.), *Solid Propellant Chemistry, Combustion, and Motor Interior Ballistics*, Vol. 185, AIAA Progress in Astronautics and Aeronautics, Washington, DC, 2000, pp. 885–906.
[19] S. Apte, V. Yang, Unsteady flow evolution in a porous chamber with surface mass injection. Part I: free oscillation, *AIAA Journal* 39 (2001) 1577–1586.
[20] W.-W. Chu, V. Yang, J. Majdalani, Premixed flame response to acoustic waves in a porous-walled chamber with surface mass injection, *Combustion and Flame* 133 (2003) 359–370.
[21] B. Ugurtas, G. Avalon, N. Lupoglazoff, F. Vuillot, G. Casalis, Stability and acoustic resonance of internal flows generated by side injection, in: V. Yang, T.B. Brill, W.-Z. Ren (Eds.), *Solid Propellant Chemistry, Combustion, and Motor Interior Ballistics*, Vol. 185, AIAA Progress in Astronautics and Aeronautics, Washington, DC, 2000, pp. 823–836.
[22] J.C. French, G.A. Flandro, J. Majdalani, Improvements to the linear standard stability prediction program (SSP), *Proceedings of the 40th AIAA/ASME/SAE/ASEE Joint Propulsion Conference*, Fort Lauderdale, FL, July 2004, Paper No. 2004-4181.
[23] J.C. French, G.A. Flandro, Linked solid rocket motor combustion stability and internal ballistics analysis, *Proceedings of the 41st AIAA/ASME/SAE/ASEE Joint Propulsion Conference*, Tuscon, AZ, July 2005, Paper No. 2005-3998.
[24] G.A. Flandro, J. Majdalani, J.C. French, Incorporation of nonlinear capabilities in the standard stability prediction program, *Proceedings of 40th AIAA Joint Propulsion Conference*, Fort Lauderdale, FL, July 2004, Paper No. 2004-4182.
[25] G.A. Flandro, S.R. Fischbach, J. Majdalani, Nonlinear rocket motor stability prediction: limit amplitude, triggering, and mean pressure shift, *Physics of Fluids* 19 (2007) 094101–094116.
[26] F.E.C. Culick, *Combustion Instabilities in Propulsion Systems*, Kluwer Academic Publishers, New York, 1996.
[27] K.W. Dotson, R.L. Baker, R.J. Bywater, Launch vehicle self-sustained oscillation from aeroelastic coupling. Part II: analysis, *Journal of Spacecraft & Rockets* 35 (1998) 374–379.
[28] J. Griffond, G. Casalis, On the nonparallel stability of the injection induced two-dimensional Taylor flow, *Physics of Fluids* 13 (2001) 1635–1644.
[29] J. Griffond, G. Casalis, On the dependence on the formulation of some nonparallel stability approaches applied to the Taylor flow, *Physics of Fluids* 12 (2000) 466–468.
[30] S.R. Fischbach, J. Majdalani, G.A. Flandro, Acoustic instability of the slab rocket motor, *Journal of Propulsion and Power* 23 (2007) 146–157.
[31] S.R. Fischbach, J. Majdalani, G.A. Flandro, Verification and validation of rocket stability integral transformations, *Proceedings of the 41st AIAA/ASME/SAE/ASEE Joint Propulsion Conference*, Tucson, AZ, July 2005, Paper No. 2005-4001.
[32] S.R. Fischbach, J. Majdalani, G.A. Flandro, Acoustic instability of the slab rocket motor, *Proceedings of the 41st AIAA/ASME/SAE/ASEE Joint Propulsion Conference*, Fort Lauderdale, FL, July 2004, Paper No. 2004-4061.
[33] J. Majdalani, G.A. Flandro, S.R. Fischbach, Some rotational corrections to the acoustic energy equation in injection-driven enclosures, *Physics of Fluids* 17 (2005) 0741020–0741021.
[34] J. Majdalani, S.R. Fischbach, G.A. Flandro, Improved energy normalization function in rocket motor stability calculations, *Journal of Aerospace Science and Technology* 10 (2006) 495–500.
[35] J. Majdalani, On steady rotational high speed flows: the compressible Taylor–Culick profile, *Proceedings of the Royal Society, London A* 463 (2006) 131–162.
[36] J. Majdalani, J. Barron, W.K. Van Moorhem, Inception of turbulence in the Stokes boundary layer over a transpiring wall, *ASME Journal of Fluids Engineering* 124 (2002) 1–7.
[37] J. Majdalani, T.S. Roh, The oscillatory channel flow with large wall injection, *Proceedings of the Royal Society, London A* 456 (2000) 1625–1657.
[38] J. Majdalani, G.A. Flandro, T.S. Roh, Convergence of two flowfield models predicting a destabilizing agent in rocket combustion, *Journal of Propulsion and Power* 16 (2000) 492–497.
[39] J. Majdalani, Improved solution for the vortical and acoustical mode coupling inside a two-dimensional cavity with porous walls, *Journal of the Acoustical Society of America* 109 (2001) 475–479.
[40] J. Majdalani, Asymptotic formulation for an acoustically driven field inside a rectangular cavity with a well-defined convective mean flow motion, *Journal of Sound and Vibration* 223 (1999) 73–95.

[41] J. Majdalani, Vortical and acoustical mode coupling inside a two-dimensional cavity with transpiring walls, *Journal of the Acoustical Society of America* 106 (1999) 46–56.
[42] J. Majdalani, The oscillatory channel flow with arbitrary wall injection, *Journal of Applied Mathematics and Physics (ZAMP)* 52 (2001) 33–61.
[43] G.A. Flandro, J. Majdalani, Aeroacoustic instability in rockets, *AIAA Journal* 41 (2003) 485–497.
[44] F. Chedevergne, G. Casalis, T. Féraille, Biglobal linear stability analysis of the flow induced by wall injection, *Physics of Fluids* 18 (2006) 014103–014114.
[45] G.A. Flandro, On flow turning, *Proceedings of the 31st AIAA/ASME/SAE/ASEE Joint Propulsion Conference*, July 1995, Paper No. 95-2730.
[46] J. Majdalani, G.A. Flandro, The oscillatory pipe flow with arbitrary wall injection, *Proceedings of the Royal Society, London A* 458 (2002) 1621–1651.
[47] J. Majdalani, The boundary layer structure in cylindrical rocket motors, *AIAA Journal* 37 (1999) 505–508.
[48] G. Kirchoff, *Vorlesungen Über Mathematische Physik: Mechanik*, second ed., Teubner, Leibzig, 1877.
[49] F.E.C. Culick, Rotational axisymmetric mean flow and damping of acoustic waves in a solid propellant rocket, *AIAA Journal* 4 (1966) 1462–1464.
[50] G.A. Flandro, J. Majdalani, Aeroacoustic instability in rockets, *Proceedings of 37st AIAA/ASME/SAE/ASEE Joint Propulsion Conference*, Salt Lake City, UT, July 2001, Paper No. 2001-3868.
[51] F.E.C. Culick, V. Yang, Prediction of the stability of unsteady motions in solid propellant rocket motors, in: L. De Luca, E.W. Price, M. Summerfield (Eds.), *Nonsteady Burning and Combustion Stability of Solid Propellants*, Vol. 143, AIAA Progress in Astronautics and Aeronautics, Washington, DC, 1992, pp. 719–779.
[52] G.A. Flandro, W. Cai, V. Yang, Turbulent transport in rocket motor unsteady flowfield, in: V. Yang, T.B. Brill, W.-Z. Ren (Eds.), *Solid Propellant Chemistry, Combustion, and Motor Interior Ballistics*, Vol. 185, AIAA Progress in Astronautics and Aeronautics, Washington, DC, 2000, pp. 837–858.